Poro-hyperelastic Anatomical Models for Hydrocephalus and Idiopathic Intracranial Hypertension

Hakseung Kim, M.Eng.,[1] Byoung-Kyong Min, Ph.D.,[1] Dae-Hyeon Park, M.Eng.,[1] Stanley Hawi, B.Eng.,[1] Byung-Jo Kim, MD/Ph.D.,[2] Zofia Czosnyka, Ph.D.,[3] Marek Czosnyka, Ph.D.,[3] Michael PF Sutcliffe, Ph.D.,[4] and Dong-Joo Kim, Ph.D.[1,*]

[1]Department of Brain and Cognitive Engineering, Korea University, Seoul, South Korea.

[2]Department of Neurology, Korea University College of Medicine, Seoul, South Korea.

[3]Department of Neurosurgery, Addenbrooke's Hospital, University of Cambridge, Cambridge, United Kingdom.

[4]Department of Engineering, University of Cambridge, Cambridge, United Kingdom.

Address correspondence to:
Dong-Joo Kim, Ph.D.
Departments of Brain and Cognitive Engineering, Korea University,
Anam-dong, Seongbu-gu, Seoul, South Korea 136-713
Phone: 0082-2-3290-5929
Fax: 0082-2-3290-3970
E-mail:dongjookim@korea.ac.kr

Key words: biomechanics; bi-phase; finite element model; hydrocephalus; idiopathic intracranial hypertension; cerebrospinal fluid;

Running head: Poro-hyperelastic models for hydrocephalus and IIH

Financial source: This research was supported by Basic Science Research Program through the National Research Foundation of Korea (NRF) funded by the Ministry of Science, ICT & Future Planning (2013R1A1A1004827), and the International Research & Development Program of the National Research Foundation of Korea (NRF) funded by the Ministry of Education, Science and Technology(MEST) of Korea(Grant number: 2014K1A3A1A21001366).

The contents of this paper have not been published.

ABSTRACT

Background: Brain deformation can be seen in hydrocephalus and idiopathic intracranial hypertension (IIH) via medical images. The phenomenology of local effects, brain shift, and raised intracranial pressure and herniation are textbook concepts. However, there are still uncertainties regarding the specific processes that occur when brain tissue is subject to the mechanical stress of different temporal and spatial profiles of the two neurological disorders. Moreover, recent studies suggest the IIH and hydrocephalus may be diseases with opposite pathogenesis. Nevertheless, the similarities and differences between the two subjects have not been thoroughly investigated.

Method: An anatomical porohyperelastic finite element model was used to assess the brain tissue responses associated with hydrocephalus and IIH. The same set of boundary conditions, with the exception of the brain loading for developing the transmantle pressure gradient, was applied for the two models. The distribution of stress and strain during the tissue distortion is described by the mechanical parameters.

Result: The results of both the hydrocephalus and IIH models correlated with pathologic characteristics. For the hydrocephalus model, periventricular oedema was associated with the presence of positive volumetric strain and void ratio in the lateral ventricle horns. By contrast, the IIH model revealed oedema across the cerebral mantle, including the centrum semiovale, with a positive void ratio and volumetric strain.

Conclusion: The model simulates all the clinical features in correlation with the MR images of hydrocephalus and IIH patients, thus providing support for the role of the transmantle pressure gradient and capillary CSF absorption in CSF-related brain deformation. The FE methods can be utilised for a better understanding of the pathophysiology of neurological disorders associated with parenchymal volumetric fluctuation.

INTRODUCTION

The disturbance in cerebrospinal fluid (CSF) dynamics is known to contribute to the distortion of the brain parenchyma[47,66]. The most well-known form of brain deformation associated with CSF disturbance is found in the hydrocephalus. Within the hydrocephalus, the obstruction in CSF circulation leads to the distortion of the brain which, in turn, produces a series of clinical symptoms including headache, nausea, vomiting and cognitive deterioration [9].

Similar concerns regarding brain deformation occur in idiopathic intracranial hypertension (IIH). IIH is a neurological disease characterised by high intracranial pressure (ICP) without apparent cause [5]. The symptoms of IIH also include headaches, but do not display any other typical signs of hydrocephalus [1]. Although the pathophysiology of IIH is largely unknown, the impaired capacity for CSF absorption is considered to be an important feature[36]. Some authors have suggested that the impaired capacity for CSF absorption in IIH may be due to resistance generated by raised venous pressure from venous outflow obstruction; however, the circumstances leading to this impairment are not yet clear[13].

Several studies suggest there may be a common physiological mechanism in IIH and hydrocephalus, but which manifests as varying pathological phenomena[2,4,27]. Winston and Breeze hypothesised that the hydraulic regulation of parenchymal volume can be explained by the pressure differences of certain entities, such as capillary pressure, ventricular fluid pressure and interstitial fluid pressure[65]. The possibility is a subject that requires further exploration. However, clinical observations or controlled trials regarding the subject would be difficult to conduct, not to mention the practical concerns thereof.

Over the past three decades, significant research[43,47,59] has been carried out to examine the biomechanics involved in the reduction of the volume of the parenchyma, or deformation of the brain tissue[59]. In particular, finite element (FE) models have been developed to investigate the biomechanical behaviour of the hydrocephalus[54]. In FE analysis, the structure is divided into numerous small elements (‘meshed’), thereby enabling numerical approximation on structural stress and deformation[69]. Since Nagashima et al[43]., first attempted to simulate the biomechanical features of the hydrocephalic brain, FE analysis of the hydrocephalic brain has been considered to be a valid approach[9,10,14,34,43,47,59,63,64,66].

This work aims to investigate the idea of the active role of the pressure gradient in brain deformation[35,47,65] associated with IIH and hydrocephalus via an FE model of the brain that is capable of simulating both disorders. The FE model would simulate characteristic features, such as brain deformation, enlarged or small ventricles,

periventricular lucency and tissue oedema, of the two disorders by manipulating transmantle pressure gradient level. In effect, the results of the present study will serve as indirect evidence for the hypothesised relationship between IIH and hydrocephalus.

METHODS

The FEM method (Abaqus/Standard, Dassault Systèmes, France) was used, as it allows for the modelling of complex domains and possesses the appropriate material properties, load histories and boundary conditions[67]. The brain geometry was taken from a set of T_2-weighted axial magnetic resonance (MR) images of a human brain, obtained from the Wolfson Brain Imaging Centre, Addenbrooke's Hospital (University of Cambridge). In order to minimise the number of clinical factors related to hydrocephalus and IIH, the image was selected from those of young, healthy adults (age = 30) who had no radiologic signs of neurological disorder. Given the symmetry of the brain in the section, only half of the slice was used.

To reduce the computational complexity caused by including sulci geometry, the model itself was constructed as a two-dimensional planar model containing the lateral ventricle and the sulci as major geometrical features. It also included various features of the exact anatomic geometry of the brain; the gray/white matter, the falx cerebri and the skull are developed as a physical part, while the outer layer of the cerebral cortex associated with the capillaries, the ependyma and the dura is represented by the interface at the boundary of the parenchyma (Figure 1).

Material properties

Peña[47] suggested three hypotheses regarding the cause of periventricular lucency, namely periventricular stress concentrations[43], CSF intrusion into the white matter due to the mechanical disruption of the ependyma[44] and the geometry (concavity of horns) of the wall[47]. There is not much evidence for the disruption of the ependyma, even though the intercellular spaces of the ependymal cells may be over-stretched or even torn, so that CSF can easily infiltrate into the periventricular tissue, according to Peña's anatomical FEM simulation[47]. Therefore, the ependymal membrane in the model is considered to be semi-permeable[15].

The falx cerebri and the skull are modelled as linear-elastic materials. The parenchyma is modelled as an isotropic, porohyperelastic theory material, containing a solid hyperelastic matrix saturated with interstitial fluid; in other

words, a porous solid having a nonlinear stress-strain relationship[6,52]. The heterogeneity of the parenchyma is addressed by assigning different properties to grey and white matter, but no additional local variations in mechanical properties of the brain are considered. Brain porosity and perfusion by CSF are implemented using a standard poroelastic consolidation theory[6]. The material properties used in the model are given in Table 1[14,32,41,43 16,30,43,50,51,57,58,61,68].

Brain loading and boundary conditions

The outer boundary of the tissue is anatomically presumed to be the capillary region, which is located in the cerebral cortex. With the support of Greitz's findings[21], it is hypothesised that interstitial fluid drains out of the capillaries. The pore pressure is set to zero along this boundary, implying a permeable boundary that allows the fluid to flow freely across the layer. In addition, this pressure provides a reference for the transmantle pressure (P_t) which, in our model, is defined as the difference between the capillary blood pressure and the ventricular fluid pressure[47].

Since the model is symmetrical, there is no horizontal displacement of the mid-line. No fluid flux occurs across the mid-line boundary, which is therefore modelled as impermeable. As a result, no prescribed pressure needs to be defined along this line. Parenchymal tissue is fixed by the falx cerebri, the end of which is firmly attached to the skull, which is itself fully constrained. There are several contact issues in the model, such as the overlapping of the meshes between adjacent entities. Self-contact was needed for the outer layer of the parenchymal tissue. Normal contact also occurs between the outer layer of the parenchymal tissue and the inner layer of the skull. Finally, contact is considered in the region between the falx cerebri and the outer layer of the parenchymal tissue (Figure 2).

The loading conditions used to model hydrocephalus and IIH were different in accordance with their differing pathophysiology. In order to produce the enlarged or small ventricles, transmantle pressure was evenly applied along the ependyma of the lateral ventricles. For the hydrocephalus model, the transmantle pressure at the lateral ventricles was set at an initial value of 0.1 mmHg. This was gradually increased to 3 mmHg over a period of 340,000 seconds (four days), as this time-span is considered the minimum period for the development of hydrocephalus [43]. In the IIH model, an initial negative ventricular fluid pressure of -3 mmHg was applied, this being lower than the capillary pressure, $P_{c,}$ in order to create an appropriate, negative pressure gradient across the cerebral mantle.

Finally, the results of the simulations were presented as four biomechanical parameters, namely the void ratio, the pore pressure, the stress and the strain. The stress combination at a given point was presented as von Mises stress. The void ratio is defined as the proportion of fluids and solids in an area. The void ratio of a normal brain is known to be 0.2[43]. Thus, a void ratio higher than 0.2 can be interpreted as an increase in fluid content, whereas a 0.2 or lower void ratio indicates a normal state or even a decrease in fluid content. The pore pressure signifies the pressure of fluid filling the pore space; a positive pore pressure indicates the inflow of fluid, whereas zero or negative pore pressure indicates being free of or an outflow of fluid. Volumetric strain is defined as the change in volume divided by the original volume[60]. When in dilation, the volumetric strain becomes positive, and vice versa. In the case of the 2-D model, two-dimensional volumetric strain was applied. The change in the volume of the z-axis was assumed to be zero.

RESULTS

Results of hydrocephalus simulation

The FEM model simulations for hydrocephalus demonstrated the core pathophysiological features of hydrocephalus, namely ventricular expansion and periventricular lucency. Figure 3A shows the model mesh before and after applying ventricular pressures of 0 mmHg and 3 mmHg.

The parameters of biological importance used proved to be good indicators for oedema mapping, as well as for the detection of ventricular expansion. From the ependymal wall analysis in Figure 4, it can be seen that there were increases in the magnitude of the void ratio of 0.65 and 0.69 at the frontal and occipital horns, respectively. Similarly, there was an increase in the volumetric strain of 0.32 and 0.34 at the frontal and occipital horns, respectively. Relatively low pore pressures of 0.6 mmHg and 1 mmHg were noted at the frontal and occipital horns, while the area adjacent to the centrum semiovale showed a much higher magnitude of 2.27 mmHg in terms of pore pressure. The von Mises stress increased by 0.93 kPa and 0.92 kPa at the frontal and occipital horns, respectively. Thus, oedema at the horns of the ventricle is simulated in relation to the features of hydrocephalus.

Ventricular expansion of the wall is demonstrated through an increase in the displacement magnitude. There was a non-uniform displacement along the ependymal wall, with a peak displacement of 19.4 mm in the centrum semiovale area adjacent to the lateral ventricle, while the frontal and occipital horns had displacements of 9.4 mm

and 12.4 mm, respectively. It was interesting to note an increase in the lengths of ependymal wall and the cerebral cortex outer layer of 28.7 mm and 14.8 mm, from their original lengths of 135 mm and 650 mm, respectively. The contour plots in Figure 5 represent the parameters of biological importance. Oedema mapping is clearly represented in Figures 5A-E.

Results of idiopathic intracranial hypertension (IIH) simulation

Both small ventricle formation and cerebral oedema presenting papilledema are simulated by our IIH model. These simulation results have similar clinical features to IIH. Figure 3B shows the model before and after ventricular pressure reduction from 0 mmHg to -3 mmHg.

The same parameters of biological importance successfully indicated cerebral oedema-affected areas, as well as the reduction of ventricle size. The ependymal wall analysis results reveal an increase in the magnitude of void ratio, volumetric strain and negative pore pressure in the area adjacent to the centrum semiovale. There was a void ratio and volumetric strain increase of 0.33 and 0.1 at the area adjacent to the centrum semiovale. Zero void ratio and negative volumetric strains of -0.66 and -0.49 are predicted at the frontal and occipital horns, respectively. Consequently, except at the frontal and occipital horns, increased tissue volume is indicated around the ventricle. A negative pore pressure (-0.09 mmHg) was also noted in the area adjacent to the centrum semiovale. As a result, there is a significant difference in these parameters at the frontal and occipital horns when compared to the area adjacent to the centrum semiovale. This indicates less accumulation of interstitial fluid at the horns compared to the centrum semiovale area. The maximum void ratio and the volumetric strain recorded at the centrum semiovale reveals oedema, and this mapping correlates with the clinical features of IIH. There were also increases in the von Mises stress at the frontal and occipital horns, with 0.57 kPa and 0.34 kPa, respectively. Small ventricle formation is revealed through a maximum inward displacement of 7 mm. We also noted an increase in the length of the ventricle ependyma of 5.7 mm from the original length of 135 mm. However, the outer layer of the cerebral cortex had no significant change in length. Contour plots in Figure 6 represent the simulation results of cerebral oedema mapping, as well as a small ventricle and compression of the brain parenchyma. Figures 5F-G and I-J represent the areas affected by cerebral oedema, while Figure 5H shows the areas that are compressed.

A direct comparison between clinical MR images shows that the important features of hydrocephalus and IIH are

simulated (Figure 6). Periventricular lucency, ventricular expansion, small ventricle, cerebral oedema and compression can be directly matched between the FEM simulation and the MR images for hydrocephalus and IIH. In addition, the parameters of biological importance used for oedema mapping (void ratio and volumetric strain) both produce reasonably accurate or identical results in comparison with the MR images (see Figure 6). For example, in the IIH model, areas of expansion due to oedema are directly correlated to the areas of expansion in the IIH model, as indicated by the arrows in Figures 6C and 6D.

DISCUSSION

Technical implication

In vivo mechanical measurements of brain material are necessarily limited. For this reason, the validation of medical hypothesis of neurological disorders involving brain deformation is often frustrating. With proper material properties and boundary conditions, the FE analysis can be an effective alternative to in-vivo measurements. There have been a number of FE analysis studies on hydrocephalic brains using various models. However, even though these linear or non-linear material models are useful for explaining aspects of hydrocephalic brain distortion, the previous models have neglected either the biphasic nature of the brain (having both solid and fluid phases) in the hyperelastic models, or the nonlinear stress-strain response of the solid phase (the neurons and neuroglia) of brain tissue in the poroelastic models[20]. For the brain material models to reflect the material properties of the brain accurately, both poroelasticity and hyperelasticity must be incorporated.

In the existing literature, the Biot model is widely used to model poroelastic structures, including the solid phase of a porous property fully saturated with a significant quantity of fluid [6,24,52]. With hyperelasticity combined, several recent studies obtained satisfactory results[20,53,59]. Furthermore, the neo-Hookean model is well suited to describing the hyperelastic, non-linear behaviour of compressible biological tissue. The model in this study is based on a recent development of the Biot model[14]. Extensions to the model are implemented by the neo-Hookean model that allows for non-linear, elastic behaviour in the solid structure. The resulting porohyperelastic model is grounded in soil mechanics, as brain tissue is a material that can be characterised by a non-linear constitutive relationship. This relationship can be then used, together with the laws of continuum mechanics, to predict the deformation response within the material due to imposed stress or displacement at the boundary. To the best of

our knowledge, the model utilised in this study is the first porohyperelastic model to incorporate complex anatomical geometry, including sulci.

Representation of the pathological features of hydrocephalus and IIH

The common features of hydrocephalus and IIH are disturbances in normal CSF circulation, which may be corrected by shunt placement[3,49]. These diseases also show intracranial hypertension. However, there are several significant differences between them. In hydrocephalus, the raised ventricular fluid pressure is the main factor contributing to intracranial hypertension via ventriculomegaly. This increased ventricular fluid pressure also exists in IIH, but is compensated for by even higher parenchymal tissue resistance, caused by cerebral edema. Thus, small ventricles are often observed in IIH. In addition, periventricular lucency is indicated for hydrocephalus, whereas diffused brain oedema is present in IIH [12,42,46].

One of the pathological features of periventricular lucency is the accumulation of a fluid, referred to as interstitial oedema, at the horns[45,47,59]. For the hydrocephalus model, a positive volumetric strain, which occurs when there is an increase in tissue volume due to fluid accumulation confirming oedema, is revealed at the frontal and occipital horns. The void ratio can be used as a good indicator for oedema[47], with areas of void expansion relating to fluid accumulation. In the hydrocephalus model, there is an increase of the void ratio to 0.61 and 0.7 at the frontal and occipital horns, respectively. The initial void ratio was taken as 0.2[43]. The results of the hydrocephalus model in this study reveal periventricular lucency providing a physical model for periventricular oedema at the frontal and occipital horns. In addition, periventricular oedema occurs even though the ependymal membrane is set to be semi-permeable.

For normal conditions in the brain, there is no significant resistance preventing fluid from flowing to the lateral ventricles[1,12,13]. However, in IIH, the transmantle pressure is nearly zero, resulting in slow fluid flow from the capillaries. This might be the reason why there is a slow progression in IIH[1]. Figure 5 shows volumetric straining, indicating cerebral oedema with the assumption that the fluid in the tissue is fully saturated, with both solid and fluid elements incompressible. In IIH, the expansion is observed adjacent to the lateral ventricles. In hydrocephalus, volumetric expansion associated with a tensile stress is shown in red. This red area is presumed to indicate cerebral oedema. Furthermore, in IIH, a significant increase in the void ratio is observed around the ventricles, while for hydrocephalus, significant expansion occurs at the frontal and occipital horns.

IIH and hydrocephalus: Opposite manifestations of disturbed CSF absorption

The proposed model demonstrated key features of brain deformation in hydrocephalus and IIH. More importantly, the model simulated and derived the results with the change in transmantle pressure gradient being the only difference between the two neurological disorders. One might expect the results of the present study to be based on false assumptions, as the issue of the transmantle pressure gradient itself is highly controversial. Some studies conclude that the transmantle pressure gradient is very small, if it exists at all[48,55]. However, a recent theoretical study also suggests that CSF-related brain deformation does not require a large pressure gradient[35]. Currently, there is no definite evidence to accept or abandon the concept of transmantle pressure gradient, which is all the more reason to construct a versatile model capable of manipulating the condition in question (Figure 7).

The brain parenchyma, when fully saturated with interstitial fluid, is incompressible or nearly incompressible. In addition, the intracranial system is encased by an effectively rigid body[40,47,59]. Therefore, enlargement of the ventricles can only occur in situations where there is volumetric reduction of the parenchyma[21,22]. This raises the question of where the drainage of interstitial fluid occurs. Previous research[23] indicates both the absorption of CSF the by brain capillaries, and that CSF is transported via vascular pulsations in the subarachnoid space (SAS). In the progression of hydrocephalus, an increase in ventricular pressure due to the disturbance in CSF absorption[11,18] induces a reversal of the pressure gradient across the cerebral mantle. Because of the high ventricular fluid pressure, the interstitial fluid pressure is higher than is the capillary pressure in hydrocephalus. Therefore, hypothetically, interstitial fluid can be wrung out of the capillaries[17,37-39,62], resulting in the volumetric reduction of brain parenchyma known as ventriculomegaly.

On the other hand, the absence of volume reduction of the parenchyma implies that no efflux of the interstitial fluid occurs through either the ventricle or the capillaries[13]. In IIH, high intraventricular pressure, as well as high capillary pressure, is commonly revealed[1,49], due to the venous stenosis[2,7,25,26,29,31]. Thus, the transmantle pressure between the two compartments (the ventricular space and capillaries) must be quite low or even negative. The low transmantle pressure associated with the resistance of extracellular channels results in difficulty in inducing the interstitial fluid's convective flux; consequently, intra-tissue water accumulation occurs, leading to an increase of ICP via water content in the brain[17,37-39,62]. This typically appears in IIH, and is viewed as vasogenic cerebral oedema of uncertain etiology, affecting the CSF pressure within the sheath of the optic nerve in relation to orbital

venous pressure[13]. Therefore, IIH-affected patients often show a degree of visual loss[19].

Capillary absorption of CSF in IIH and hydrocephalus

The conventional view of CSF dynamics states that most, if not all, CSF is absorbed at the superior sagittal sinus via arachnoid granulation[8]. While this may explain how hydrocephalus can develop, it does not provide a clear explanation regarding the development of IIH. Meanwhile, the model in this study is based on recent theories and the discovery that a significant amount of CSF is absorbed in the capillary region[21] and will later drain out through the venous sinuses [2,7,25,26,29,31]. With this modified view of CSF dynamics, the reason that impaired CSF absorption manifests as hydrocephalus or IIH can be considered.

Since the ventricular fluid pressure is elevated in both diseases, the differentiating factor would be the capillary pressure, which is heavily affected by venous outflow. In hydrocephalus, the ventricular fluid pressure increases due to the blockage at the arachnoid granulation. The high transmantle pressure gradient causes the efflux of interstitial fluid to the capillary; thus, the brain deforms with ventriculomegaly. On the contrary, in IIH, the capillary pressure becomes elevated due to venous stenosis. This causes a low or even negative transmantle pressure gradient and no efflux of interstitial fluid into the capillary, subsequently inducing the accumulation of interstitial fluid at the brain parenchyma. This then causes intracranial hypertension, due to cerebral oedema without ventriculomegaly. In addition, a similar mechanism may lead to SVS in shunted patients, as hypothesised and documented in earlier studies[2,28]. In summary, the FE model used in this study correlates in many aspects with the clinical features of the two major neurological disorders associated with CSF-related brain deformation. The results of the model support the concept of the transmantle pressure gradient as a major factor in CSF-related brain deformation. The clinical application of the FE brain model will help to anticipate the pathogenesis of space-occupying lesions in the brain. In reality, various reasons for inducing fluctuations in transmantle pressure gradients should be considered in order to fully explain the varying degrees of brain deformation. This may help to provide better prognoses on an individual patient basis and could be applicable for the treatment of patients that is more tailored in the future.

CONCUSION

The proposed 2-D finite element model of the head has suggested the mechanisms of the development of both hydrocephalus and IIH. Specifically, periventricular lucency and ventricular enlargement correlated with the clinical results for hydrocephalus. Cerebral oedema presenting papilledema in IIH was also demonstrated using the model. Our results seem to support the hypothesis that IIH and hydrocephalus, as CSF-absorption related neurological disorders, are diseases with opposite pathogenesis and that the reabsorption of interstitial fluid in the capillaries is a key mechanism for the phenomena.

ACKNOWLEDGEMENT

We are grateful to Dr. R. Jena (Dept. of Oncology) and Dr. J. Pickard (Dept. of Neurosurgery), both from Addenbrooke's Hospital, Cambridge

DISCLOSURE

The authors report no conflict of interest concerning the materials or methods used in this study or the findings specified in this paper.

APPENDIX

Derivation of 2-D model from MR image

MR images were processed using ScanIP (Simpleware Software Ltd, U.K) to obtain brain cross-sections that allow the region of interest (i.e. the brain) to be segmented. From these sections, ScanFe (Simpleware software Ltd, U.K) made it possible to produce a 3D finite element mesh of the sliced brain and to export the model in a form compatible with Abaqus.

With the selected work flow of the geometric model, deriving a 2D model from the 3D finite element mesh was not trivial. The MR source images contain voxels that represent thickness while the desired 2D model has no thickness. Thus to get the 2D model from the 3D Abaqus input file derived from ScanFE, in house FORTRAN codes were developed and used. The 2D surface of the extracted model has a relatively poor mesh quality. Hypermesh (Altair Engineering, USA), a pre-processing software, was used to remove errors, repair mesh elements, build in the surface of the model and, ultimately, to export the model for performing an Abaqus FEM analysis.

A finite element mesh was generated with 4-node quadrilateral elements using an automated mesh generating algorithm. For the simulations, a plane strain model is used to represent a slice of the brain and skull. The changes in geometry in the out-of-plane direction are considered to be sufficiently gentle to make such an approximation reasonable. An alternative 2D approach would be to adopt an axisymmetric model, but the geometry, especially around the frontal and occipital horns of lateral ventricle, would no longer be effectively represented.

The material properties and derivation of field equations

The model used reduced-integration Abaqus elements CPE4RP (four-node bilinear displacement and pore pressure, reduced integration with hourglass control), CPS4R (four-node bilinear, reduced integration with hourglass control) CPE4R (four-node bilinear, reduced integration with hourglass control) and CPE3 (three-node, linear) for the parenchymal tissue, the skull and the falx cerebri, respectively. The total number of elements in the model is around 18,000. Abaqus 6.12-3 non-linear element code was used with implicit time integration associated with soil and hyper elastic analysis, accounting for both the constitutive and geometric non linearity.

Poro-hyperelastic models for hydrocephalus and IIH

The major difference between poro-hyperelastic model (which this study utilized) and previous model comes from the assumption on material property of the brain parenchyma. The porohyperelastic model describes the brain as hyperelastic solid matrix, saturated with interstitial fluid [6,52]. The Young's modulus of the brain parenchyma was adopted from existing study[41]. Considering the compressibility of the solid matrix of the parenchyma, Poisson's ratio was set as 0.35 [14,32,43]. The material properties of the rest compartments of the model, i.e. the falx cerebri and skull are considered as linear-elastic materials. Thus, the material properties (Young's modulus, density and Poisson's ratio) of these compartments came from previous studies [16,30,33,50,51,57,58,61] (Figure A-1)

The material response is the combination of neo-Hookean hyper-elastic and volumetric porous material models, simulated using Abaqus 6.12. According to the Abaqus user manual[56] , the strain energy potential U for the compressible neo-Hookean material model) is of the form

$$U = C_{10}(\bar{I}_1 - 3) + \frac{1}{D_1}(J-1)^2, \ (\because J_{el} = \frac{J}{J_{th}}, \ J_{th} = (1+e_{th})^3) \qquad \text{Eq. (1)}$$

where, J_{el} is the elastic volume ratio; J_{th} is the thermal volume ratio; e_{th} is the linear thermal extension; $\bar{I}_1$ is the measure of the distortion in the material; and C_{10} and D_1 are material parameters. The C_{10} parameter describes the shear behavior of the material, and the D_1 parameter introduces compressibility. The tissue material is compressible; thus D_1 should not be zero. The initial shear modulus, μ_0 , and bulk modulus, K_0 , are given by

$$\mu_0 = 2C_{10} \ \text{ and } \ K_0 = \frac{2}{D_1} \qquad \text{Eq. (2)}$$

Based on the above relationships, we can calculate C_{10} and D_1 from typical material properties (i.e. Young's modulus and Poisson's ratio.

The porous material model can be expressed in the form of $\sigma = \mu f(\varepsilon)$ where the function of ε is non-linear and μ is a normalizing parameter. The porosity was obtained by using Forchheimer's law. This can be written as

$$f = -\frac{k}{\gamma_w}\left(\frac{\partial u_w}{\partial x} - \rho_w g\right) \qquad \text{Eq. (3)}$$

where, f is volumetric flow rate, k is permeability, γ_w is wetting fluid specific weight, u is wetting fluid pore pressure, x is position, ρ_w is wetting fluid density and g is gravity.

REFERENCE

1. Ball AK, Clarke CE: Idiopathic intracranial hypertension. **Lancet Neurol 5:**433-442, 2006
2. Bateman GA: Hypertensive slit ventricle syndrome: pseudotumor cerebri with a malfunctioning shunt? **J Neurosurg 119:**1503-1510, 2013
3. Bateman GA, Loiselle AM: Can MR measurement of intracranial hydrodynamics and compliance differentiate which patient with idiopathic normal pressure hydrocephalus will improve following shunt insertion? **Acta Neurochir (Wien) 149:**455-462, 2007
4. Bateman GA, Smith RL, Siddique SH: Idiopathic hydrocephalus in children and idiopathic intracranial hypertension in adults: two manifestations of the same pathophysiological process? **J Neurosurg Pediatr 107:**439-444, 2007
5. Binder DK, Horton JC, Lawton MT, McDermott MW: Idiopathic intracranial hypertension. **Neurosurgery 54:**538-552, 2004
6. Biot MA: General Theory of Three-Dimensional Consolidation. **J Appl Phys 12:**155, 1941
7. Bono F, Giliberto C, Mastrandrea C, Cristiano D, Lavano A, Fera F, et al: Transverse sinus stenoses persist after normalization of the CSF pressure in IIH. **Neurology 65:**1090-1093, 2005
8. Brodbelt A, Stoodley M: CSF pathways: a review. **Br J Neurosurg 21:**510-520, 2007
9. Cheng S, Bilston LE: Computational model of the cerebral ventricles in hydrocephalus. **J Biomech Eng 132:**054501, 2010
10. Clatz O, Litrico S, Delingette H, Paquis P, Ayache N: Dynamic model of communicating hydrocephalus for surgery simulation. **IEEE Trans Biomed Eng 54:**755-758, 2007
11. Dandy WE: Extirpation of the Choroid Plexus of the Lateral Ventricles in Communicating Hydrocephalus. **Ann Surg 68:**569-579, 1918
12. Dessardo NS, Dessardo S, Sasso A, Sarunic AV, Dezulovic MS: Pediatric idiopathic intracranial hypertension: clinical and demographic features. **Coll Antropol 34:**217-221, 2010
13. Dhungana S, Sharrack B, Woodroofe N: Idiopathic intracranial hypertension. **Acta Neurol Scand 121:**71-82, 2010
14. Dutta-Roy T, Wittek A, Miller K: Biomechanical modelling of normal pressure hydrocephalus. **J Biomech 41:**2263-2271, 2008
15. Ebinger M: Core topics in neuroanesthesia and neurointensive care. **Arch Neurol 69:**788-789, 2012

16. FA B, Rolf HE: Three-dimensional finite element analysis of the human brain under combined rotational and translational accelerations. Paper presented at the 38th Stapp Car Crash Conference, Fort Lauderdale, FL, USA, 1994

17. Fishman RA: Experimental obstructive hydrocephalus: Changes in the cerebrum. **Arch Neurol 8:**156-161, 1963

18. Fode NC, Laws ER, Sundt TM: Communicating hydrocephalus after subarachnoid hemorrhage: results of shunt procedures. **J Neurosurg Nurs 11:**253-256, 1979

19. Friedman DI, Jacobson DM: Diagnostic criteria for idiopathic intracranial hypertension. **Neurology 59:**1492-1495, 2002

20. Garcia JJ, Smith JH: A biphasic hyperelastic model for hydrocephalus **Latin Am Appl Res 40:**295-323, 2010

21. Greitz D: Cerebrospinal fluid circulation and associated intracranial dynamics. A radiologic investigation using MR imaging and radionuclide cisternography. **Acta Radiol Suppl 386:**1-23, 1993

22. Greitz D: Radiological assessment of hydrocephalus: new theories and implications for therapy. **Neurosurg Rev 27:**145-165, 2004

23. Greitz D, Greitz T, Hindmarsh T: A new view on the CSF-circulation with the potential for pharmacological treatment of childhood hydrocephalus. **Acta Paediatr 86:**125-132, 1997

24. Hakim S, Venegas JG, Burton JD: The physics of the cranial cavity, hydrocephalus and normal pressure hydrocephalus: mechanical interpretation and mathematical model. **Surg Neurol 5:**187-210, 1976

25. Higgins JN, Gillard JH, Owler BK, Harkness K, Pickard JD: MR venography in idiopathic intracranial hypertension: unappreciated and misunderstood. **J Neurol Neurosurg Psychiatry 75:**621-625, 2004

26. Higgins JN, Owler BK, Cousins C, Pickard JD: Venous sinus stenting for refractory benign intracranial hypertension. **Lancet 359:**228-230, 2002

27. Iencean SM: Idiopathic intracranial hypertension and idiopathic normal pressure hydrocephalus: diseases with opposite pathogenesis? **Medical Hypotheses 61:**526-528, 2003

28. Jang M, Yoon SH: Hypothesis for intracranial hypertension in slit ventricle syndrome: new concept of capillary absorption laziness in the hydrocephalic patients with long-term shunts. **Medical Hypotheses 81:**199-201, 2013

29. Janny P, Chazal J, Colnet G, Irthum B, Georget AM: Benign intracranial hypertension and disorders of

CSF absorption. **Surg Neurol 15:**168-174, 1981

30. Jiroušek O, Jíra J, Jírová J, Micka M: Finite Element Model of Human Skull Used for Head Injury Criteria Assessment, in Gilchrist MD (ed): **IUTAM Symposium on Impact Biomechanics: From Fundamental Insights to Applications**. Netherlands: Springer, 2005, pp 459-467
31. Johnston I, Hawke S, Halmagyi M, Teo C: The pseudotumor syndrome. Disorders of cerebrospinal fluid circulation causing intracranial hypertension without ventriculomegaly. **Arch Neurol 48:**740-747, 1991
32. Kaczmarek M, Subramaniam RP, Neff SR: The hydromechanics of hydrocephalus: steady-state solutions for cylindrical geometry. **Bull Math Biol 59:**295-323, 1997
33. Kupczik K, Dobson CA, Fagan MJ, Crompton RH, Oxnard CE, O'Higgins P: Assessing mechanical function of the zygomatic region in macaques: validation and sensitivity testing of finite element models. **J Anat 210:**41-53, 2007
34. Lefever JA, Garcia JJ, Smith JH: A patient-specific, finite element model for noncommunicating hydrocephalus capable of large deformation. **J Biomech 46:**1447-1453, 2013
35. Levine DN: Intracranial pressure and ventricular expansion in hydrocephalus: have we been asking the wrong question? **J Neurol Sci 269:**1-11, 2008
36. Levine DN: Ventricular size in pseudotumor cerebri and the theory of impaired CSF absorption. **J Neurol Sci 177:**85-94, 2000
37. Lux We: Periventricular water content: Effect of pressure in experimental chronic hydrocephalus. **Arch Neurol 23:**475-479, 1970
38. MClone DG, Bondareff W, Raimondi AJ: Brain edema in the hydrocephalic hy-3 mouse: submicroscopic morphology. **J Neuropath Exp Neurol 30:**627-637, 1971
39. Milhorat TH, Clark RG, Hammock MK: Experimental hydrocephalus. 2. Gross pathological findings in acute and subacute obstructive hydrocephalus in the dog and monkey. **J Neurosurg 32:**390-399, 1970
40. Miller K, Chinzei K, Orssengo G, Bednarz P: Mechanical properties of brain tissue in-vivo: experiment and computer simulation. **J Biomech 33:**1369-1376, 2000
41. Miller K, Taylor Z, Nowinski WL: Towards computing brain deformations for diagnosis, prognosis and neurosurgical simulation. **J Mech Med Biol 5:**105-121, 2005
42. Nadkarni T, Rekate H: Treatment of refractory intracranial hypertension in a spina bifida patient by a concurrent ventricular and cisterna magna-to-peritoneal shunt. **Childs Nerv Syst 21:**579-582, 2005

43. Nagashima T, Tamaki N, Matsumoto S, Horwitz B, Seguchi Y: Biomechanics of hydrocephalus: a new theoretical model. **Neurosurgery 21:**898-904, 1987

44. Naidich TP, Epstein F, Lin JP, Kricheff II, Hochwald GM: Evaluation of Pediatric Hydrocephalus by Computed Tomography. **Radiology 119:**337-345, 1976

45. O'Hayon BB, Drake JM, Ossip MG, Tuli S, Clarke M: Frontal and occipital horn ratio: A linear estimate of ventricular size for multiple imaging modalities in pediatric hydrocephalus. **Pediatr Neurosurg 29:**245-249, 1998

46. Olivero WC, Rekate HL, Chizeck HJ, Ko W, McCormick JM: Relationship between intracranial and sagittal sinus pressure in normal and hydrocephalic dogs. **Pediatr Neurosci 14:**196-201, 1988

47. Pena A, Bolton MD, Whitehouse H, Pickard JD: Effects of brain ventricular shape on periventricular biomechanics: a finite-element analysis. **Neurosurgery 45:**107, 1999

48. Penn RD, Lee MC, Linninger AA, Miesel K, Lu SN, Stylos L: Pressure gradients in the brain in an experimental model of hydrocephalus. **J Neurosurg 102:**1069-1075, 2005

49. Rekate HL: Hydrocephalus and idiopathic intracranial hypertension. **J Neurosurg Pediatr 107:**435-438, 2007

50. Ruan JS, Khalil T, King AI: Human head dynamic response to side impact by finite element modeling. **J Biomech Eng 113:**276-283, 1991

51. Sarkar S, Majumder S, Roychowdhury A: Response of human head under static and dynamic load using finite element method. **Trends Biomater Artif Organs 17:**130-134, 2004

52. Simon BR: Multiphase poroelastic finite element models for soft tissue structure. **Appl Mech Rev 45:**191-218, 1992

53. Smith JH, García JJ: A Nonlinear Biphasic Hyperelastic Model for Acute Hydrocephalus. Paper presented at the ASME 2008 Summer Bioengineering Conference, Marco Island, Florida, USA, June 25-29, 2008

54. Sobey I, Wirth B: Effect of non-linear permeability in a spherically symmetric model of hydrocephalus. **Math Med Biol 23:**339-361, 2006

55. Stephensen H, Tisell M, Wikkelso C: There is no transmantle pressure gradient in communicating or noncommunicating hydrocephalus. **Neurosurgery 50:**763-773, 2002

56. Systèmes D (ed): **Abaqus 6.12 Theory Manual**. Providence: Dassault Systèmes Simulia Corp, 2012

57. Takhounts EG, Eppinger RH, Campbell JQ, Tannous RE, Power ED, Shook LS: On the Development of the SIMon Finite Element Head Model. **Stapp Car Crash J 47:**107-133, 2003

58. Takhounts EG, Ridella SA, Hasija V, Tannous RE, Campbell JQ, Malone D, et al: Investigation of traumatic brain injuries using the next generation of simulated injury monitor (SIMon) finite element head model. **Stapp Car Crash J 52:**1-31, 2008

59. Taylor Z, Miller K: Reassessment of brain elasticity for analysis of biomechanisms of hydrocephalus. **J Biomech 37:**1263-1269, 2004

60. Wang H (ed): **Theory of linear poroelasticity with applications to geomechanics and hydrogeology**. Princeton: Princeton University Press, 2000

61. Watanabe D, Yuge K, Nishimoto T, Murakami S, Takao H: Impact Injury Analysis of the Human Head. **ATZautotechnology 7:**34-37, 2007

62. Weller RO, Wisniewski H: Histological and ultrastructural changes with experimental hydrocephalus in adult rabbits. **Brain 92:**819-828, 1969

63. Wilkie KP, Drapaca CS, Sivaloganathan S: Aging impact on brain biomechanics with applications to hydrocephalus. **Math Med Biol 29:**145-161, 2012

64. Wilkie KP, Drapaca CS, Sivaloganathan S: A theoretical study of the effect of intraventricular pulsations on the pathogenesis of hydrocephalus. **Appl Math Comput 215:**3181-3191, 2010

65. Winston KR, Breeze RE: Hydraulic regulation of brain parenchymal volume. **Neurol Res 13:**237-247, 1991

66. Wirth B, Sobey I: An axisymmetric and fully 3D poroelastic model for the evolution of hydrocephalus. **Math Med Biol 23:**363-388, 2006

67. Wu JZ, Herzog W, Epstein M: Evaluation of the finite element software Abaqus for biomechanical modelling of biphasic tissues. **J Biomech 31:**165-169, 1998

68. Yoganandan N (ed): **Frontiers in Head and Neck Trauma: Clinical and Biomechanical.** Amsterdam: IOS Press, 1998

69. Zienkiewicz OC, Taylor RL (ed): **The finite element method 4th ed.** New York: McGraw-Hill, 1989

FIGURE LEGENDS

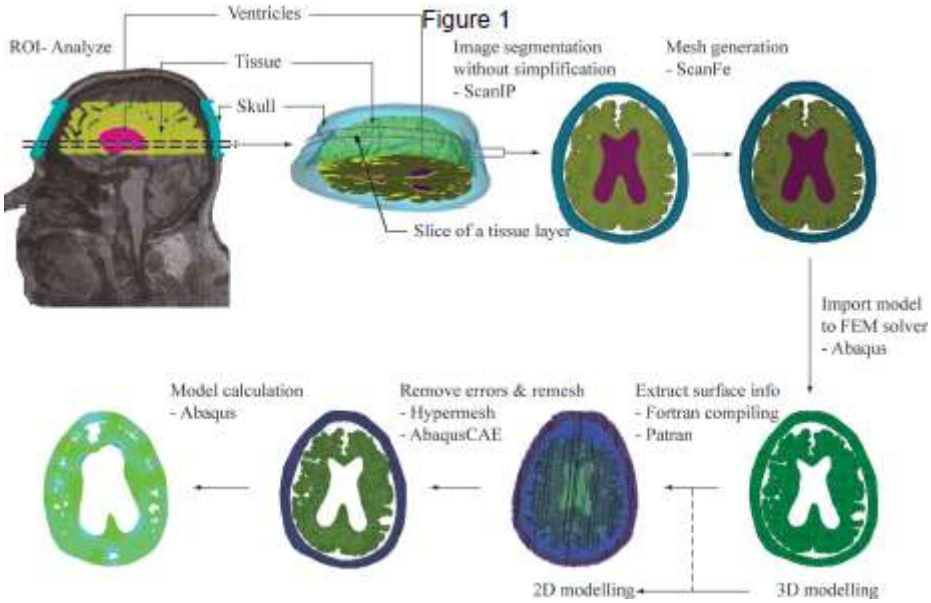

Figure 1 Overview of the model's development. T2-weighted axial magnetic resonance images (MRI) of a healthy human brain were processed using ScanFE to produce a 3-D mesh. FORTRAN codes were developed to turn a 3-D Abaqus model into a 2-D model. Hypermesh (Altair Engineering, USA), a pre-processing software, was used to remove errors and to replace mesh elements. For the detailed process of deriving the model from the MR image, please refer to the APPENDIX.

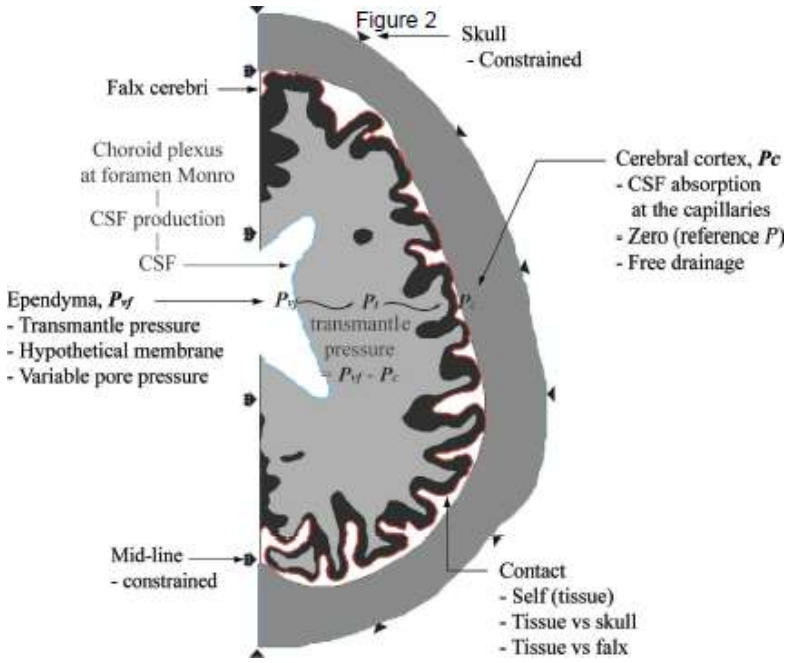

Figure 2 Schematic illustrations of the load and boundary conditions. The load and boundary conditions applied in the FEM model, the ventricle and capillaries, have prescribed pressures, the skull is fully constrained and the mid-line boundary is constrained against the x-direction displacement. The outer boundary of the parenchyma is assumed to be the capillaries, where the interstitial fluid drains out.

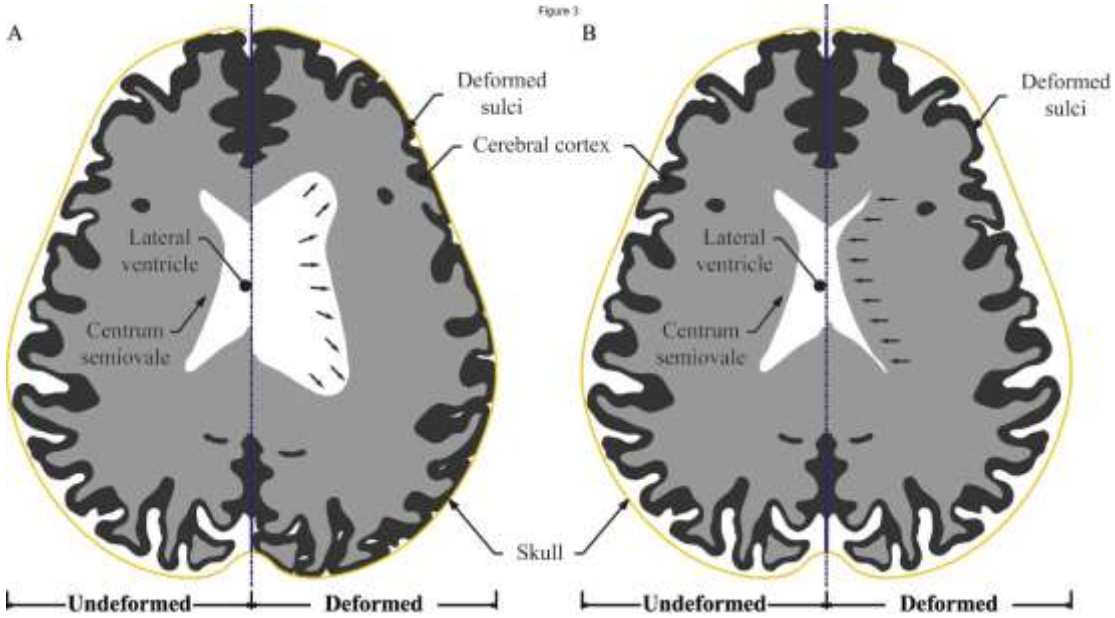

Figure 3 Undeformed versus deformed models of the hydrocephalus and IIH. (A) Undeformed and deformed hydrocephalus finite model simulation, illustrating the ventricular dilation and sulci deformation, (B) Undeformed and deformed IIH finite element model simulation illustrating small ventricle formation and the expansion of the periventricular tissue.

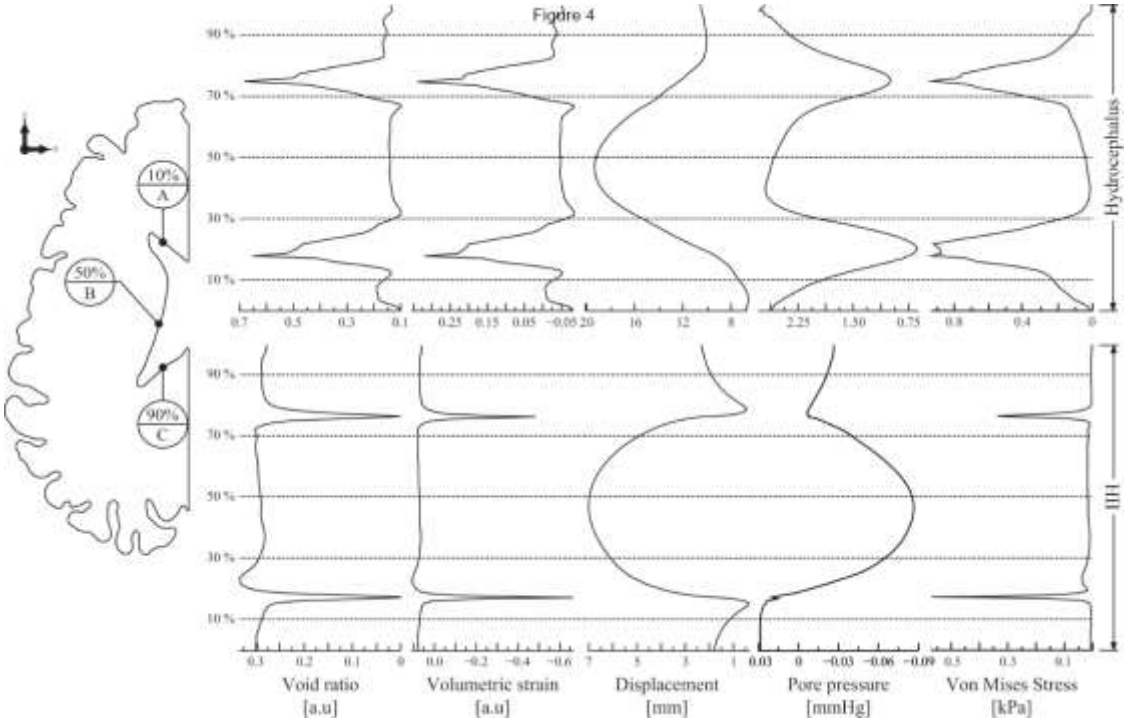

Figure 4 Ependymal wall analysis comparison of the lateral ventricle. The hydrocephalus (bottom) and IIH (top) were simulated by using five key parameters, namely void ratio, volumetric strain, displacement (mm), pore pressure (mmHg) and von Mises stress (kPa). The percentages from 0% to 100% represent the normalised distance along the ependymal wall of the lateral ventricle.

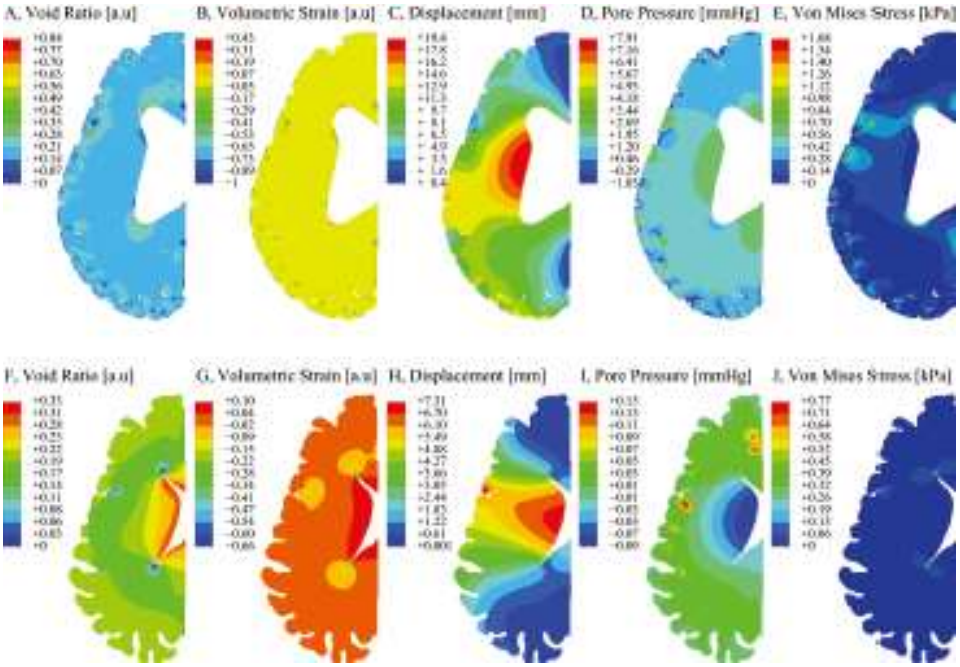

Figure 5 Contour plot representations: The plots of the void ratio, volumetric strain, displacement, pore pressure and von Mises stress from the FEM simulation results for hydrocephalus (top) and IIH (bottom).

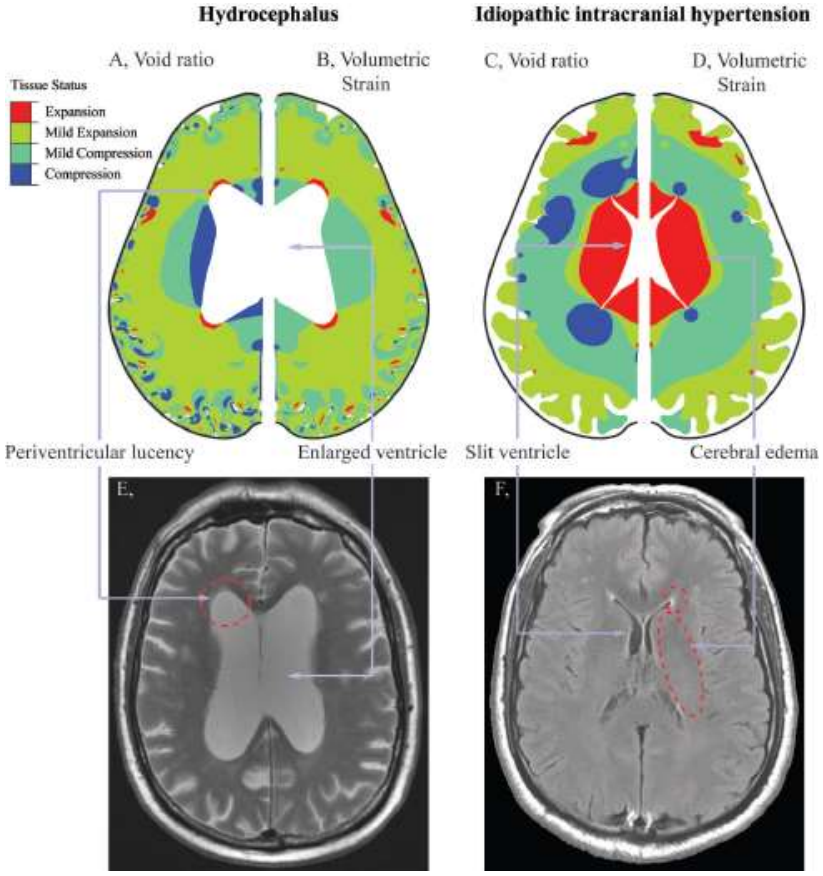

Figure 6 Comparison of clinical MR images and FEM simulation results. Mild expansion and mild compression are presumed to be equal to 10% of the maximum expansion and compression. Void ratio and volumetric strain similarities as oedema mapping indicators are illustrated.

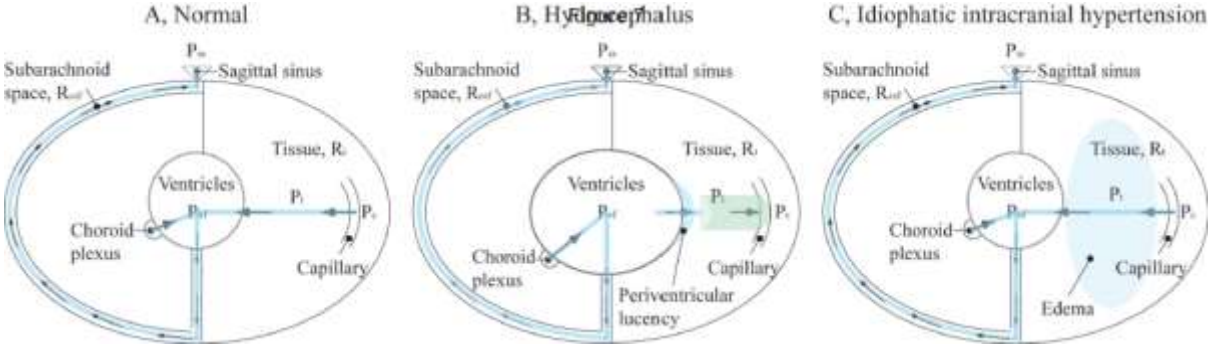

Figure 7 Schematic diagram of the physiology of (A) normal, (B) hydrocephalus and (C) idiopathic intracranial hypertension. P_c= Capillary pressure, P_t = Transmantle pressure and P_{vf} = Ventricular fluid pressure. R_t = Tissue resistance, and P_{ss} = Sagittal sinus pressure. In hydrocephalus, $P_c < P_{vf}$ due to the disturbed CSF absorption, thus resulting in positive P_t. The increased P_t forces the interstitial fluid to flow to the capillaries, which allows ventriculomegaly. On the other hand, in IIH, the P_c becomes higher due to venous stenosis, leading to a very small or even negative transmantle pressure gradient level. This enables the accumulation of ISF in the parenchyma, thus resulting in hypertension, often with small ventricles, although it remains high P_{vf}.

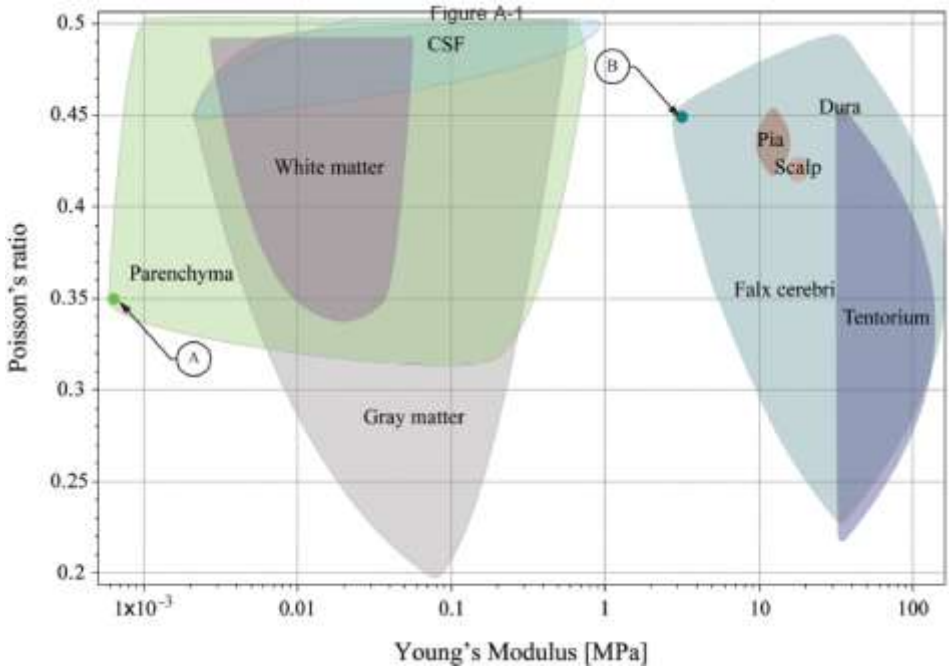

Figure A-1 Graphical representation of known value of Young's modulus and Poisson's ratio on various intracranial entities. The dots A, B indicates the values used in this study.

TABLE 1 Summary of the material properties; C01 and D1 are calculated from E and v and the details of the calculations can be found in the Appendix.

Parenchyma				Falx cerebri			
E_p [Pa]	v_p	C_{01} [Pa]	D_1 [Pa]	E_f [Pa]	V_f	ρ_f [kgm^{-3}]	t [mm]
420	0.35	77.9	224	3.4×10^6	0.45	1130	2
e	ρ_p [kgm^{-3}]	k [m/s]		Skull			
0.2	1040	WM	1×10^{-7}	E_s [Pa]	v_s	ρ_s [kgm^{-3}]	
		GM	1×10^{-9}	14×10^9	0.23	1412	

N.B. E_p is Young's modulus of parenchyma [15,43]; v_p is Poisson's ratio of parenchyma [34,46,50]; k is permeability [34]; e is void ratio [46]; ρ_p is density of parenchyma; E_f is Young's modulus of falx cerebri [32,59]; v_f is Poisson's ratio of falx cerebri [32,70]; t is the thickness [70]; ρ_f is density of falx cerebri [70]; E_s is Young's modulus of skull [32,59]; v_f is Poisson's ratio of skull [32,70]; ρ_s is density of skull [70]